

EQUIVALENT MULTI-TISSUE AND THERMODYNAMIC DECOMPRESSION ALGORITHMS

B. R. WIENKE

Applied Theoretical Physics Division, Los Alamos National Laboratory, Los Alamos, NM 87545 (U.S.A.)

(Received March 17th, 1989)

(Revision received June 19th, 1989)

(Accepted June 19th, 1989)

Multi-tissue and thermodynamic decompression algorithms are described and a computational equivalence is established between the two approaches. Eigenvalues and weighted eigenfunctions of the Fick-Fourier equation effectively define response functions from which Haldane half-lives can be extracted from arbitrary exposures, operationally bridging the two approaches. Decompression criteria for the algorithms are also described and coupled. Comparisons of similarities and differences of approaches are given from both theoretical and applied viewpoints. A seven-parameter set, spanning both models, forms the basis of analysis. We find that representative thermodynamic parameters in a perfusion-diffusion model effectively recover Haldane half-lives in a bootstrap and that critical parameters overlap, though ranges differ in the two cases.

Keywords: Decompression; Mathematical models; Tissue gas exchange; Critical parameters; Multi-tissue supersaturation; Phase equilibration; Perfusion-diffusion transport

Introduction

Models based on supersaturation [1—7] and phase equilibrium [7—11] are employed in decompression applications, even though exchange equations, staging criteria, and test correlations differ. Computational algorithms also track the same data sets with differing implementations. Such being the case, we bridge implementations of multi-tissue and thermodynamic algorithms by relating eigenvalues and eigenfunctions of the Fick-Fourier equation to multi-tissue response functions of the Haldane equation. Time scales in both algorithms are contrasted for choices of model parameters. Tissue diffusivities, D , and perfusion rates, κ , in a perfusion-diffusion framework are employed to estimate gas tensions for ranges of exposures, and the resulting tensions are then inverted to estimate the usual Haldane half-lives, τ . For short time intervals, a Haldane-like approximation to the perfusion-diffusion exchange equations is suggested by requiring continuity of response functions and their first derivatives, and the same asymptotic behavior at late time. Critical (dissolved gas) tensions, M , and thermodynamic (separated gas) fractions, χ , are also related for multi-tissue compartments. Procedurally, the overlap is exhibited over sets of depth-time exposures.

In contrasting these algorithms, basic assumptions and mathematical techniques are also described [12,13]. An algorithm simply consists of a set of inert gas exchange equations and staging criteria for arbitrary exposures, the application of which is central to the fabrication of decompression tables and meter software. It is well known that perfusion and diffusion parameters employed in most algorithms are not strongly correlated [14—17] with measured critical tissue values. Some of this is due to model limitations in describing gas transport and phase mechanics, that is, equations must be stretched to support dynamics outside algorithm range and model framework. But even given these caveats, a basic commonality between the two algorithms can be demonstrated in applications, the delineation of which is hopefully timely and unambiguous. We underscore the overlap in computational terms, focusing on the tissue exchange equations and staging criteria. Sections 2 and 3 detail the multi-tissue and thermodynamic algorithms and computational bases. Section 4 details the operational equivalences which can be erected between the two models. A parameter set involving λ , M , D , κ , and χ is employed in the synthesis. A cursory discussion of tissue gas exchange models and equations will facilitate development before addressing specifics.

Tissue is separated into intravascular and extravascular regions for modeling. Blood containing dissolved inert and metabolic gases passes through the intravascular zone, providing both initial and boundary conditions for subsequent gas transport through the extended extravascular zone. Arterial blood first equilibrates with alveolar partial pressures, and venous blood then equilibrates with arterial tensions at a somewhat slower rate. Tissue tensions fall somewhere between arterial and venous tensions during equilibration. Three equations are applied to model transport, namely, a diffusion equation, a perfusion rate equation, and a combined perfusion-diffusion equation. Defining the instantaneous gas tension, p , given any constant tension, p_0 , with the relative difference, $\Pi = p - p_0$, the diffusion equation is given by,

$$\nabla \cdot (D\nabla)\Pi = \frac{\partial\Pi}{\partial t}, \quad (1-1)$$

with ∇ the spatial gradient operator, t the time, and D the diffusion coefficient. The arbitrary tension, p_0 , can always be chosen to yield homogeneous initial or boundary conditions, that is, $\Pi = 0$ initially, or on the boundary [13]. The perfusion rate equation for gas exchange is similarly written,

$$\frac{\partial\Pi}{\partial t} = -\lambda\Pi, \quad (1-2)$$

for λ some characteristic time constant for buildup, or decay. Solutions to Eqn. (1-2), depending only on the initial condition, are independent of position in tissue, obviously a simplification that requires rapid intercellular gas diffusion compared to time scales on the order of λ^{-1} . When diffusion, perfusion, and metabolic assimilation are included in the balance, the transport equation generalizes to the Fick-Fourier expression.

$$\nabla \cdot (D\nabla)\Pi = \frac{\partial\Pi}{\partial t} + \kappa\Pi + Z(\Pi), \quad (1-3)$$

with Z the metabolic consumption rate and κ a perfusion time constant. For inert gases, obviously $Z = 0$. Solutions to Eqn. (1-3) depend on both initial and boundary conditions, with simplification afforded in the homogeneous case, as with solutions to Eqn. (1-1). Clearly, the Fick-Fourier expression contains the diffusion and perfusion rate equations as limiting subsets. It will be convenient to express ambient pressures, P , in units of feet-of-sea water (fsw), and gas partial pressures, p , as mole fractions of ambient pressure.

Multi-tissue Algorithm

The multi-tissue algorithm is based on a bulk perfusion equation. Classical and modern multi-tissue approaches [1,18] to decompression are based on assumptions of limited supersaturation, with the transport of matter across regions of varying concentration, or pressure, driven by the local gradient, and gas uptake and elimination limited by blood flow rates. As discussed, the rate equation is given by Eqn. (1-2), with λ a set of phenomenological (tissue) constants. Denoting initial tension, p_i , we have,

$$\Pi(0) = p_i - p_a = \Pi_i, \quad (2-1)$$

and integrating Eqn. (1-2) subject to the above yields,

$$p - p_a = (p_i - p_a) \exp(-\lambda t). \quad (2-2)$$

The time for $p - p_a$ to decrease to half its immediate value, after reduction in p_a , is the tissue half-life, τ ,

$$\tau = \frac{\ln 2}{\lambda}. \quad (2-3)$$

As many as ten (hypothetical) compartments with 2.5, 5, 10, 20, 40, 80, 120, 180, 240 and 360 min half-lives are employed in applications, and half-lives, τ , are routinely assigned to be independent of p_a . Compartments are just computational entities, and direct anatomical linkages are neither intended nor implied. Much detail is obviously buried in these tissue parameters, since they are not correlated with critical tissue equilibration rates [8]. Given absolute pressure, P , multi-tissue theory postulates that the degree to which any compartment tolerates nitrogen saturation is limited by a critical ratio, R ,

$$\frac{p}{P} \leq R, \quad (2-4)$$

having a modern range, $1.10 \leq R \leq 3.20$, popularized by the US Navy. Realistically,

R depends on many factors, not always discernible. Alternatively, the values of p for which the equalities hold in Eqns. (2.13) and (2-4) are the critical tensions, M . The correlated critical pressures collected by Buhlmann [5] and Workman [18] for specific compartments at various depths, as well as the later phenomenological compilation of Schreiner [19] and VGE analysis of Spencer [20] provide a staging criteria. Surfacing ratios, R_0 , critical pressures, $M_0 = R_0 P_0$, and depth ratios, R_∞ ($d \rightarrow \infty$), are shown in Table I for six compartments. As a function of altitude, z , measured in feet, atmospheric pressure, P_0 , is conveniently represented [6] by the barometer-like expression,

$$P_0 = 33 \exp(-\xi z), \quad (2-5)$$

with,

$$\xi = 0.38119 \times 10^{-4} \text{ ft}^{-1}. \quad (2-6)$$

The extension of the critical surface pressures and ratios in Table I to altitude has been a study in itself [4,5]. Linear [4] and exponential [6] extrapolations of the critical pressures back to zero have been proposed. A few-parameter fit [6] to the critical pressures, expressed as linear functions of absolute pressure, also suggests that critical pressures vary inversely as the fourth root of the compartment half-life, τ , as seen in Fig. 1. The fit to the surfacing tensions, M_0 , takes the form,

$$M_0 = 155 \tau^{-0.25}, \quad (2-7)$$

as tabulated in the fourth column of Table I. Surfacing critical tensions, M_0 , correspond to near saturation exposures at depth, d_0 ,

$$d_0 = 1.265 M_0 - 33. \quad (2-8)$$

The critical ratios are larger for faster tissues and lesser pressures, yet range of variation is not large, especially within compartments. Blood rich, well-perfused,

TABLE I

SURFACING AND DEPTH RATIOS, CRITICAL AND FITTED NITROGEN PRESSURES ($P_0 = 33$ fsw)

τ (min)	R_0	M_0 (fsw)	$155 \tau^{-0.25}$ (fsw)	R_∞
5	3.15	104	104	2.27
10	2.67	88	87	2.01
20	2.18	72	73	1.67
40	1.76	58	60	1.34
80	1.58	52	52	1.26
120	1.55	51	49	1.19

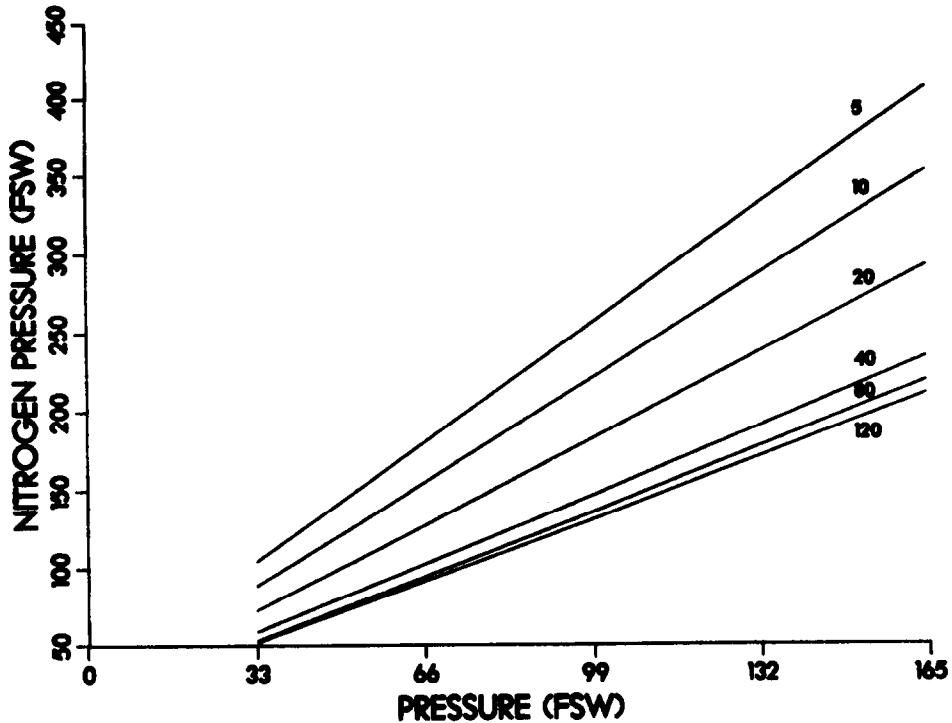


Fig. 1. Critical tensions and half-lives.

aqueous tissues are usually assumed to be *fast* (small values of τ), while blood poorer, scarcely-perfused, lipid tissues are assumed to be *slow* (large values of τ). The multi-tissue model addresses dissolved gas exchange, with saturation gradients driving the interchange between blood and tissue. In the presence of free phases, exchange-mechanisms outside the multi-tissue model framework are enabled [7,11,17]. Free-dissolved and free-blood gradients can compete with dissolved-blood gradients. If gas nuclei are entrained in the circulatory system, blood perfusion rates are effectively lowered, an impairment with impact on all gas exchange processes.

Thermodynamic Algorithm

Questions of whether perfusion or diffusion are rate limiting in tissue, whether bounded or bulk models are sufficiently representative for decompression analyses, how are free-dissolved gas interactions quantified, and why are seemingly dissimilar models successful in applications, prompted studies with a broader kinetic perspective. Thermodynamic models are an offspring of such studies, culminating in a number of algorithm approaches [3,7,9,10]. An approach, suggested by Hills [11] and extended by Hennessy [8], is more comprehensive than multi-tissue treatments,

addressing a number of additional issues. This thermodynamic algorithm is based on phase equilibration of dissolved and separated gases, with uptake and elimination of inert gas limited by perfusion and diffusion. From a boundary (vascular) zone of thickness, a , gases diffuse into the cellular region. Cylindrical, one-dimensional, symmetry, as seen in Fig. 2, is assumed in the extended zone [16]. The radial diffusion equation, given by Eqns. (1-1) and (1-3), is subject to the boundary conditions,

$$\begin{aligned} \Pi(x, 0) &= p_i - p_v = \Pi_i, \\ \Pi(a, t) &= p_v - p_v = 0, \\ \frac{\partial \Pi(c, t)}{\partial r} &= \frac{\partial (p - p_v)}{\partial r} = 0. \end{aligned} \quad (3-1)$$

with the venous tension, p_v , a time-dependent quantity linking blood flow rate and gas solubility to the mass flux across the vascular boundary according to a balance equation. The derivative boundary condition at $c = b/2$ imparts reflection symmetry to the spatial solution. Accordingly, separating variables in Eqn. (1-1) and solving, we write,

$$p - p_v = (p_i - p_v)R(r, t), \quad (3-2)$$

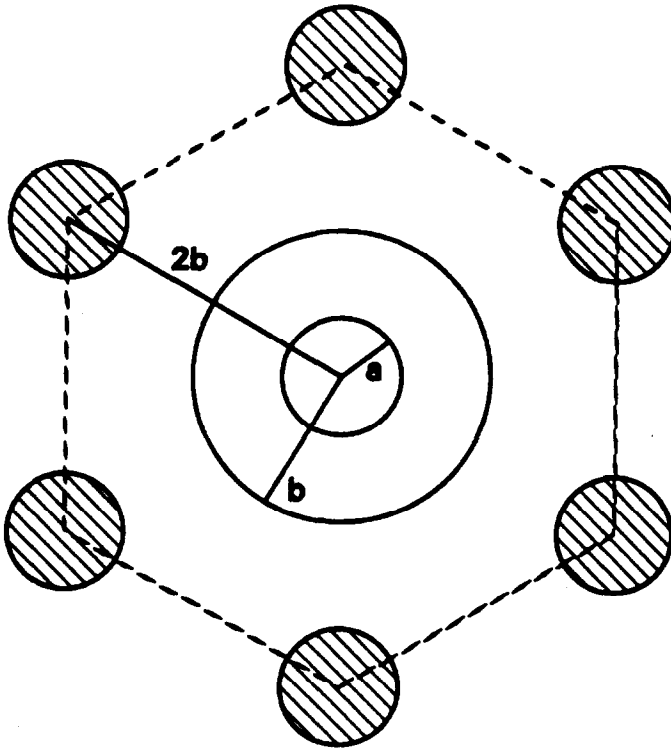


Fig. 2. Cylindrical tissue geometry.

for,

$$R(r, t) = \pi \sum_{n=1}^{\infty} \frac{J_1^2(\beta_n c)}{[J_0^2(\beta_n a) - J_1^2(\beta_n c)]} U_0(\beta_n r) \exp(-\beta_n^2 D t) = \sum_{n=1}^{\infty} R_n(r, t). \quad (3-3)$$

with U_0 defined in Eqn. (2-2), and the derivative boundary condition at the mid-point, $r = c$, requiring,

$$J_0(\beta_n a) Y_1(\beta_n c) - Y_0(\beta_n a) J_1(\beta_n c) = 0. \quad (3-4)$$

for which the eigenvalues, β_n , are the roots of the zonal equation. The transport model also assumes a fully-stirred extended vascular zone from which venous blood leaves in equilibrium with respect to all gases, while arterial blood either diminishes or replenishes gases in the zone. Perfusion-limiting is applied as a boundary condition through the time-varying venous tension, p_v , by enforcing a mass balance across both the vascular and cellular regions at $r = a$, with $\Pi_v = p_v - p_a$

$$S_b \frac{\partial \Pi_v}{\partial t} = -\kappa S_b \Pi_v - \frac{3}{a} S_c D \left[\frac{\partial \Pi}{\partial r} \right]_{r=a}, \quad (3-5)$$

for κ a perfusion time constant, S_c and S_b the nitrogen cellular and blood solubilities, and p_a the arterial gas tension. Clearly, Eqns. (3-2) and (3-5) bootstrap the tissue tension, p , venous tension, p_v , and arterial tension, p_a , in a complex feedback loop. Hennessy [8] has shown that the solution to the coupled set, Eqns. (3-3), (3-4), and (3-5), in various limits contains the solutions to all deterministic models hitherto described for gas exchange. In a few paragraphs, an analytic solution to the Fick-Fourier equation will be presented that has common features with the thermodynamic approach, but is easier to contrast with the multi-tissue algorithm because only one exchange equation with appropriate boundary conditions is employed.

One can couple the volume of separated gas, v , to mass balance under worse-case conditions. With cellular solubility, S_c in tissue volume, V , the mass balance, with zero gas elimination, is given by,

$$v P_{N_2} = V S_c [p - P_{N_2}], \quad (3-6)$$

which states that the amount of separated gas is the difference between the original amount of nitrogen in solution before decompression and the amount left in solution. Employing the perfusion boundary tension, p_v , the balance equation takes the form,

$$\chi P_{N_2} = S_c [p_v + (p_i - p_v) \bar{R}(t) - P_{N_2}], \quad (3-7)$$

with $\chi = v/V$, and the spatially-averaged response function given by,

$$\bar{R}(t) = \frac{4}{(b^2 - a^2)} \sum_{n=1}^{\infty} \frac{1}{\beta_n^2} \frac{J_1^2(\beta_n c)}{[J_0^2(\beta_n a) - J_1^2(\beta_n c)]} \exp(-\beta_n^2 D t) = \sum_{n=1}^{\infty} \bar{R}_n(t), \quad (3-8)$$

which permits evaluation of the separated gas fraction, χ , for arbitrary exposures provided the partial pressure, P_{N_2} , is known. Both are limited for the phase algorithm in the following way.

Hills [11] proposed a criteria for decompression pain based on pressure differentials between separated gas and surrounding tissue. If the pressure differential, δ , exceeds a critical threshold, δ' , pain occurs,

$$\delta > \delta', \quad (3-9)$$

or, equivalently, by Boyle's law with tissue modulus, K ,

$$K\chi \geq \delta', \quad (3-10)$$

with critical thresholds in the range,

$$0.43 \leq \delta' \leq 1.13 \text{ fsw}. \quad (3.11)$$

These thresholds correspond to separated gas fractions, employing a nominal value [10] for K ,

$$0.0039 \leq \chi \leq 0.0093, \quad (3-12)$$

which are small, yet not insignificant. The identification of the separated gas fraction, χ , as a critical indicator is a significant development. Hennessy and Hemplemann [9] established a linear titration curve between saturation and safe decompression pressures, assuming that the same critical volume of released gas provokes mild attacks of decompression sickness. Their analysis also offers explanations for changes in signs and symptoms which follow changes in the nature of the exposure to pressure. Similarly, Yount and Hoffman [21] linked separated gas volumes in a bubble formation model to establish decompression criteria.

While inert gas tensions vary dramatically with depth, oxygen, carbon dioxide, and water vapor tensions are fairly constant under normal conditions. Worse-case, separated nitrogen pressure, P_{N_2} , as a function of ambient pressure is also suggested by Hills [11],

$$P_{N_2} = P + 3.21 \text{ fsw}. \quad (3-13)$$

Here separated nitrogen takes up the difference between total hydrostatic pressure and the sum of metabolic gas and water vapor pressures. Arterial nitrogen equilibrates with alveolar nitrogen in less than a minute. At equilibrium, the nitrogen tissue, p , venous, p_v , and arterial, p_a , tensions are all equal to the alveolar partial pressure, P_{N_2} , which can be written, accounting for water vapor dilution (1.61 fsw),

$$p_{N_2} = 0.79P - 1.61 \text{ fsw}, \quad (3-14)$$

taking 0.79 as the nitrogen mole fraction. The pressure difference, Δ , between ambient pressure and the sum of dissolved gases is the biological *inherent unsaturation*, [10], or the *oxygen window* [3],

$$\Delta = P - p_{O_2} - p_{CO_2} - p_{H_2O} - p_{N_2} = 0.21P - 3.85 f_{sw}, \quad (3-15)$$

taking the sum of dissolved and separated oxygen, water vapor, and carbon dioxide to be the same, according to Hills [10],

$$p_{O_2} + p_{CO_2} + p_{H_2O} = 5.47 f_{sw}. \quad (3-16)$$

The unsaturation occurs because carbon dioxide produced by metabolism is more soluble in tissue than oxygen consumed and exerts a lower partial pressure.

The Fick-Fourier algorithm employs Eqn. (1-3), which is the diffusion equation with a perfusion term, $\kappa\Pi$, included. The presence of the perfusion term will force all tensions to approach the arterial tension, p_a , over long time scales, that is, $\Pi = p - p_a = 0$ when time derivatives and diffusion gradients vanish. A time-dependent boundary condition, mocking up the mass balance constraint, Eqn. (3-5), can also be introduced to account for relaxation times between venous and arterial tensions. The algorithm parallels the thermodynamic formulation in many respects, as seen accordingly.

From the vascular boundary, gases diffuse into the cellular zone according to the Fick-Fourier equation. Planar, one-dimensional symmetry, is assigned in the extended zone. We first change variables under the substitution,

$$\Pi = U \exp(-\kappa t) \quad (3-17)$$

with perfusion constant, κ , defined,

$$\kappa = f\mu, \quad (3-18)$$

for f the blood-tissue fraction and μ the perfusion rate. The initial and boundary conditions, allowing venous tensions at the boundaries to relax to arterial tensions at some rate, σ , possibly slower than the perfusion rate due to flow considerations ($\sigma \leq \kappa$), are taken to be,

$$\begin{aligned} \Pi(x, 0) &= p_i - p_a = \Pi_i, \\ \Pi(a, t) &= (p_v - p_a) \exp(-\sigma t) = \Pi_0 \exp(-\sigma t), \\ \Pi(b, t) &= (p_v - p_a) \exp(-\sigma t) = \Pi_0 \exp(-\sigma t), \end{aligned} \quad (3-19)$$

constituting an inhomogeneous set. These boundary conditions attempted to emulate a mass-balanced (average) tissue tension. Substituting Eqn. (3-17) into Eqn. (1-3) to eliminate the perfusion term, yields a diffusion equation for U in plane geometry,

$$D \frac{\partial^2 U}{\partial x^2} = \frac{\partial U}{\partial t}, \quad (3-20)$$

with initial and boundary conditions,

$$\begin{aligned} U(x, 0) &= \Pi_i \\ U(a, t) &= \Pi_0 \exp[(\kappa - \sigma)t] \\ U(b, t) &= \Pi_0 \exp[(\kappa - \sigma)t]. \end{aligned} \quad (3-21)$$

The general method of Duhamel [12] can be invoked to solve Eqns. (3-20) and (3-21). The solution, U , is broken into two parts, X and W ,

$$U = X + W, \quad (3-22)$$

with associated boundary conditions

$$\begin{aligned} X(x, 0) &= \Pi_i \\ X(a, t) &= 0 \\ X(b, t) &= 0 \end{aligned} \quad (3-23)$$

and,

$$\begin{aligned} W(x, 0) &= 0 \\ W(a, t) &= \Pi_0 \exp[(\kappa - \sigma)t], \\ W(b, t) &= \Pi_0 \exp[(\kappa - \sigma)t], \end{aligned} \quad (3-24)$$

for a dual set of diffusion equations,

$$D \frac{\partial^2 X}{\partial x^2} = \frac{\partial X}{\partial t} \quad D \frac{\partial^2 W}{\partial x^2} = \frac{\partial W}{\partial t}. \quad (3-25)$$

Unlike the previous case, the tissue, arterial, and venous tensions are not bootstrapped by separate mass balance and transport equations, obviously a numerical simplification. Solving Eqns. (3-23) through (3-26) and multiplying the solution U by $\exp(-\kappa t)$ according to Eqn. (3-17) yields,

$$p - p_a = (p_v - p_a)G(x, t) + (p_i - p_a)H(x, t), \quad (3-26)$$

for,

$$\begin{aligned}
 G(x, t) &= \sum_{n=1}^{\infty} \frac{4}{(b-a)} \frac{\alpha_{2n-1} D}{(\alpha_{2n-1}^2 D + \kappa - \sigma)} \sin[\alpha_{2n-1}(x-a)] \\
 &\quad \times [\exp(-\sigma t) - \exp(-\alpha_{2n-1}^2 D t - \kappa t)] \\
 &= \sum_{n=1}^{\infty} G_{2n-1}(x, t), \\
 H(x, t) &= \sum_{n=1}^{\infty} \frac{4}{(2n-1)\pi} \sin[\alpha_{2n-1}(x-a)] \exp(-\alpha_{2n-1}^2 D t - \kappa t) \\
 &= \sum_{n=1}^{\infty} H_{2n-1}(x, t), \tag{3-27}
 \end{aligned}$$

and eigenvalues, α defined by,

$$\alpha_{2n-1} = \frac{(2n-1)\pi}{(b-a)}. \tag{3-28}$$

Obviously for large perfusion and/or diffusion rates, the response function decays very rapidly in time. The perfusion terms, $\exp(-\kappa t)$ and $\exp(-\sigma t)$, multiply the sum of Fourier diffusion components. But, because only a single equation is employed, perfusion and diffusion are not sequenced in a two-step process, as in the preceding thermodynamic treatment. The analytic form is not only easier to handle numerically, it also permits direct coupling to the multi-tissue algorithm, as will be seen in Section 4.

Denoting the *vascularity*, $\epsilon = a/b$, the blood-tissue partition coefficient, f , from Eqn. (5-19) is taken [8,11] in this model,

$$\begin{aligned}
 f &= \frac{S_b}{S_b \epsilon^2 + (1 - \epsilon^2) S_c} = \frac{1}{\epsilon^2 + (1 - \epsilon^2) S_p}, \\
 S_p &= \frac{S_c}{S_b}, \tag{3-29}
 \end{aligned}$$

for S_b (0.0125 atm^{-1}) and S_c (0.069 atm^{-1}) blood and cellular nitrogen solubilities, and typical ratios, $S_p \approx 1$ for aqueous tissue, $S_p \approx 5$ for lipid tissue. Vascularity, ϵ , has the range, $1/15 \leq \epsilon \leq 1/5$, so that for most applications, $f = 1/S_p$. The balance equation takes the analogous form to Eqn. (3-7),

$$\chi P_{N_2} = S_c [p_a + (p_v - p_a) \bar{G}(t) + (p_i - p_a) \bar{H}(t) - P_{N_2}], \tag{3-30}$$

with averaged response functions given by,

$$\begin{aligned} \bar{G}(t) &= \frac{8}{(b-a)^2} \sum_{n=1}^{\infty} \frac{D}{(\alpha_{2n-1}^2 D + \kappa - \sigma)} [\exp(-\sigma t) - \exp(-\alpha_{2n-1}^2 D t - \kappa t)] \\ &= \sum_{n=1}^{\infty} \bar{G}_{2n-1}(t), \\ \bar{H}(t) &= \frac{8}{\pi^2} \sum_{n=1}^{\infty} \frac{1}{(2n-1)^2} \exp(-\alpha_{2n-1}^2 D t - \kappa t) = \sum_{n=1}^{\infty} \bar{H}_{2n-1}(t). \end{aligned} \tag{3-31}$$

The functions, \bar{H} and \bar{G} , broadly reflect diffusion and perfusion exchange in opposite limits, though effects get folded together by virtue of decaying exponentials involving both κ and D . Exchange is clearly perfusion-controlled whenever $\alpha_{2n-1}^2 D \gg \kappa$, and then $\bar{H} < \bar{G}$. But, when $\alpha_{2n-1}^2 D \ll \kappa$, diffusion can compete with $\bar{H} > \bar{G}$. To give a better feeling for the net effects of κ and D on the exchange, consider the lowest order ($n = 1$) terms in the expansion given by,

$$\begin{aligned} \bar{G}(t) &\approx \frac{8}{(b-a)^2} \frac{D}{\alpha_1^2 D + \kappa - \sigma} [\exp(-\sigma t) - \exp(-\alpha_1^2 D t - \kappa t)], \\ \bar{H}(t) &\approx \frac{8}{\pi^2} \exp(-\alpha_1^2 D t - \kappa t). \end{aligned} \tag{3-32}$$

For large D ,

$$\begin{aligned} \bar{G}(t) &\rightarrow \frac{8}{\pi^2} \exp(-\sigma t), \\ \bar{H}(t) &\rightarrow 0, \end{aligned} \tag{3-33}$$

while for small D ,

$$\begin{aligned} \bar{G}(t) &\rightarrow \frac{8}{(b-a)^2} \frac{D}{\alpha_1^2 D + \kappa - \sigma} [\exp(-\sigma t) - \exp(-\kappa t)], \\ \bar{H}(t) &\rightarrow \frac{8}{\pi^2} \exp(-\kappa t) \end{aligned} \tag{3-34}$$

so that the response depends on D for small D , and on κ and σ for large D . When D and κ are of similar magnitude, perfusion and diffusion bootstrap each other, with neither one or the other predominating.

The average tissue tension, \bar{P} , in a circulation-limited (perfusion) exchange satisfies the mass balance [14,15], with $\bar{\Pi} = \bar{P} - p_\sigma$

$$S_c \frac{\partial \bar{\Pi}}{\partial t} = -S_b \kappa \bar{\Pi}, \tag{3-35}$$

similar in structure to Eqn. (3-5). Integrating, and applying the initial condition that,

$$\bar{\Pi}(x, 0) = p_v - p_a = \bar{\Pi}_i, \quad (3-36)$$

yields,

$$\bar{p} - p_a = (p_v - p_a) \exp(-\sigma t), \quad (3-37)$$

with,

$$\sigma = \frac{S_b}{S_c} \kappa. \quad (3-38)$$

Since,

$$\frac{S_b}{S_c} = \frac{1}{S_p} \leq 1. \quad (3-39)$$

one has in general,

$$\sigma \leq \kappa. \quad (3-40)$$

The boundary conditions, Eqns. (3-19), thus impose mass balance through the mean tension, \bar{P} .

Algorithm Equivalence

Opposing limits of \bar{G} and \bar{H} suggest that effective half-lives, τ can be defined which depend inversely on D and κ , that is, considering only the lowest order diffusion term ($n = 1$),

$$\tau = \tau_D + \tau_\kappa, \quad (4-1)$$

with,

$$\begin{aligned} \tau_D &= \frac{\ln 2}{\alpha_1^2 D}, \\ \tau_\kappa &= \frac{\ln 2}{\kappa}. \end{aligned} \quad (4-2)$$

exhibiting the limiting form as $D \rightarrow \infty$,

$$\tau \rightarrow \frac{\ln 2}{\kappa} \quad (4-3)$$

or as $\kappa \rightarrow \infty$,

$$\tau \rightarrow \frac{\ln 2}{\alpha_1^2 D} \quad (4-4)$$

Implicit to Eqn. (4-1) is an approximate time scale for gas penetration that adds separate diffusion and perfusion time scales together, though the response function, Eqn. (3-31), includes boundary effects from the relaxation parameter, σ . Still one reasonably expects that σ and κ are of the same magnitude so that the approximation scale remains valid. Higher order diffusion terms, that is terms with $n \gg 1$, damp out rapidly in the response function. Thus in opposite extremes, τ is bounded by diffusion or perfusion time scales. In between, effects interfere, as first noted by Hennessy [8] and Hills [11]. Tables II and III contrast lipid and aqueous half-lives for various values of $\theta = D/a^2$, and f , fixing $\epsilon = 1/5$ for illustration, and taking the lowest order diffusion term, $n = 1$. Values of $\theta = D/a^2$ represent the two extremes of homogeneous (water) and heterogeneous (cellular) diffusion, that is $D \approx 10^{-5} \text{ cm}^2 \text{ s}^{-1}$ and $D \approx 10^{-10} \text{ cm}^2 \text{ s}^{-1}$. In the last columns, the perfusion half-lives, τ_κ , are also listed for contrast.

For small θ , both perfusion and diffusion contribute to τ , while for larger θ only perfusion matters in both Tables. An overlap between τ and τ_κ , is clearly exhibited for smaller values of the perfusion, μ , in all of the above cases. Accepting the water (tissue) value of $\theta = 10^4 \text{ min}^{-1}$, perfusion would be the controlling mechanism for gas uptake and elimination. The set of half-lives, τ , (5, 10, 20, 40, 80, 120, 180, 240, 360 min), employed in the multi-tissue algorithm are recovered from Tables II and III in the perfusion range, $0.001 \leq \mu \leq 1.0 \text{ min}^{-1}$, for $\theta = 10^4 \text{ min}^{-1}$, but a requisitely broader range for $\theta = 10^{-1} \text{ min}^{-1}$. For small value of the diffusivity, θ , and large perfusion μ , diffusion is rate-limiting. Effective half-lives for aqueous tissue are five times faster than their lipid counterparts for large θ , but decrease from a maximum of five times their lipid values at very small perfusion, μ , to approximate equality at large perfusion μ , for small θ . For quick comparison, Table IV gives the perfusion rates, μ , required by Eqns. (3-18) and (3-29) for the standard set of half-

TABLE II

AQUEOUS TISSUE HALF-LIVES AND PERFUSION-DIFFUSION SPECTRUM ($\epsilon = 1/5$, $S_p = 1$)

μ (min ⁻¹)	τ (min)		τ_κ (min)
	$\theta = 10^{-1}$ (min ⁻¹)	$\theta = 10^4$ (min ⁻¹)	
0.0001	6942.7	6931.4	6931.5
0.0010	704.4	693.1	693.2
0.0100	80.6	69.3	69.3
0.1000	18.2	6.9	6.9
1.000	11.9	0.7	0.7
10.00	11.3	0.07	0.07
100.0	11.2	0.007	0.007

TABLE III

LIPID TISSUE HALF-LIVES AND PERFUSION-DIFFUSION SPECTRUM ($\epsilon = 1/5, S_p = 5$)

μ (min ⁻¹)	τ (min)		τ_κ (min)
	$\theta = 10^{-1}$ (min ⁻¹)	$\theta = 10^4$ (min ⁻¹)	
0.0001	33559.0	33548.0	33548.0
0.0010	3366.0	3354.8	3354.8
0.0100	346.7	335.4	335.5
0.1000	44.8	33.5	33.5
1.000	14.6	3.4	3.4
10.00	11.6	0.34	0.34
100.00	11.2	0.034	0.034

lives, τ , and $\epsilon = 1/5$ in lipid and aqueous tissue. Lipid and aqueous perfusion rates vary by a constant factor, $f = 4.84$, for $\epsilon = 1/5$. For a given value of κ which recovers τ , there are any number of values of μ , ϵ , and S_p according to Eqns. (3-18) and (3-29).

Having described exchange models, decompression criteria, and time scales, we now apply algorithms to a set of arbitrary exposures and quantitatively delineate the overlap using parameters such as λ , D , κ , and σ , as well as M , d' , and χ . This seven-parameter set constitutes a basis for many deterministic algorithms. The corresponding sets of perfusion, μ , in lipid and aqueous tissue, computed in Table IV for the standard set of multi-tissue half-lives, are pertinent by virtue of their widespread effective use in table and meter fabrication. The well-known $t^{1/2}$ law for bounce exposures to depth, d , originally suggested by Hempleman [2], and later modified by Spencer [20], offers a simple time scale to compare algorithms,

$$dt^{1/2} \leq 475 fsw \text{ min}^{1/2}. \quad (4-5)$$

TABLE IV

PERFUSION RATES AND HALF-LIVES FOR LIPID AND AQUEOUS TISSUE ($\epsilon = 1/5$)

τ (min)	κ (min ⁻¹)	μ (min ⁻¹)	
		$S_p = 1$	$S_p = 5$
5	0.13863	0.13863	0.67096
10	0.06931	0.06931	0.33546
20	0.03466	0.03466	0.16775
40	0.01733	0.01733	0.08387
80	0.00866	0.00866	0.04191
120	0.00578	0.00578	0.02797
180	0.00385	0.00385	0.01863
240	0.00289	0.00289	0.01398
360	0.00193	0.00193	0.00934

TABLE V

MULTI-TISSUE AND THERMODYNAMIC HALF-LIVES ($\theta = 10^{-1} \text{ min}^{-1}$)

τ (min)	d (ft)						
	30	50	80	110	140	170	200
5	5.5	5.5	5.4	5.3	5.2	5.2	5.1
10	11	11	11	10	10	10	10
20	22	22	21	21	20	20	20
40	44	43	42	41	40	38	37
80	88	86	83	79	75	72	68
120	130	130	120	110	110	100	93
180	200	190	180	160	150	140	120
240	260	250	240	210	190	170	150
360	390	370	330	290	250	220	190

Using Eqns. (3-26) and (3-31) to compute tissue tensions at depths, d , for bounce exposures limited by Eqn. (4-5) and κ given in Table IV, Tables V and VI compare multi-tissue half-lives obtained by equating Eqn. (2-1) to Eqn. (3-26) and then inverting to estimate λ and τ for each κ . In Tables V and VI, values of θ vary as before, that is, $\theta = 10^{-1} \text{ min}^{-1}$, and $\theta = 10^4 \text{ min}^{-1}$. For added simplicity, we also take $\varphi = (p_v - p_a)/p_i - p_a = 0.9$ and $\sigma = 0.9 \kappa$. Equation (3-29) are again employed to estimate f . In the summation over diffusion terms in Eqns. (3-31), 25 terms ($n = 1, 25$) are used. The standard set, τ , is listed in column one and the inverted values, obtained from the perfusion-diffusion equations, are compared in the remaining columns for exposures in roughly 30 ft increments.

For the same κ as given in Table IV, the inverted half-lives of Tables V and VI clearly overlap the standard set in a range which grows larger as the half-lives increase, regardless of the value of the diffusivity, θ . Computationally, this means that both Eqns. (2-2) and (3-26) track similar depth-time exposures, limited simply by Eqn. (4-5) for quoted ranges of parameters. For fast tissues, the relative spread is

TABLE VI

MULTI-TISSUE AND THERMODYNAMIC HALF-LIVES ($\theta = 10^4 \text{ min}^{-1}$)

τ (min)	d (ft)						
	30	50	80	110	140	170	200
5	5.6	5.6	5.5	5.5	5.5	5.5	5.5
10	11	11	11	11	11	11	10
20	22	22	22	22	22	21	21
40	44	44	44	43	42	41	40
80	88	88	86	83	80	76	72
120	130	130	120	110	110	100	99
180	200	190	180	170	160	150	130
240	260	260	240	220	200	180	160
360	390	380	340	290	260	230	200

TABLE VII

CRITICAL TENSIONS AND SEPARATED GAS FRACTIONS

τ (min)	M_0 (fsw)	d_0 (ft)	t_0 (min)	χ aqueous	χ lipid
5	103.6	98.2	23.4	0.0220	0.1215
10	87.2	77.3	37.7	0.0158	0.0875
20	73.3	59.7	63.1	0.0104	0.0576
40	61.6	45.0	111.3	0.0067	0.0371
80	51.8	32.6	212.2	0.0036	0.0200
120	46.8	26.3	326.6	0.0020	0.0121
180	42.3	20.6	533.4	0.0010	0.0055
240	39.4	16.8	794.8	0.0003	0.0018
360	35.6	12.0	1555.6	0.0001	0.0010

small, obviously increasing, though, as τ grows large. As τ grows larger, the perfusion rates, κ , drop, and diffusive terms affect calculations. At any rate, since the standard set, τ , is arbitrary, another set, μ , κ , ϵ , S_p , and θ can always be *interfitted* as far as predicting the same tensions, p . In passing, it should also be noted that the calculations, particularly the overlapping structures of the half-life spectra, are sensitive to σ and φ . Values of $\sigma < 0.6 \kappa$ and $\varphi < 0.7$ do not recover the standard set, τ , in the bootstrap. With equivalenced tissue functions, we next turn to the decompression criteria, M , and χ .

Each compartment, τ , has a critical surfacing tension, M_0 , corresponding to near saturation exposure at depth, d_0 , according to Eqns. (2-7) and (2-8). For bounce exposures, time limits, t_0 , can be estimated from Eqn. (4-5). Using Eqn. (2-2) to predict the multi-tissue tensions at the bounce limits, t_0 , and Eqn. (3-13) to estimate the worse-case free phase pressures, P_N , Eqn. (3-6) can then be employed to extract the separated fractions, χ , implicit to the critical tensions, M_0 . Table VII lists M_0 , d_0 , t_0 , and χ for both aqueous ($S_b = 0.0125 \text{ atm}^{-1}$) and lipid ($S_c = 0.069 \text{ atm}^{-1}$) cases. Aqueous compartments slower than 20 min satisfy the criteria, Eqn. (3-12), but only lipid compartments slower than 120 min are compatible. Given the arbitrariness of the M -value construction, this not too surprising. Yet, broad overlap is seen. A similar equivalence between the separated fraction, χ , and the decompression data over a much broader exposure range, including altitude, has been described by Hills [10,11]. The fact that the faster compartments, τ , with larger critical tensions corresponding to deeper exposures, do not agree with the phase criteria, Eqn. (3-12), is to be expected. Elimination gradients in the supersaturation and phase models are fundamentally different [11,17], and such differences are reflected in M and χ .

In closing, we give a simpler representation for Eqns. (3-26) and (3-31) which can be employed numerically for small exponential arguments. The tissue function, Eqn. (3-26), can be approximated,

$$p - p_a = (p_i - p_a) \sum_{n=1}^{\infty} \omega_{2n-1} \exp(-\lambda_{2n-1} t), \quad (4-6)$$

by equating expressions and their first derivatives at $t = 0$,

$$\begin{aligned}
 [(p - p_a)]_{t=0} &= \sum_{n=1}^{\infty} \omega_{2n-1} = (p_v - p_a) \sum_{n=1}^{\infty} \bar{G}_{2n-1}(0) + (p_i - p_a) \sum_{n=1}^{\infty} \bar{H}_{2n-1}(0), \\
 \left[\frac{\partial(p - p_a)}{\partial t} \right]_{t=0} &= - \sum_{n=1}^{\infty} \omega_{2n-1} \lambda_{2n-1} \\
 &= (p_v - p_a) \sum_{n=1}^{\infty} \frac{\partial \bar{G}_{2n-1}(0)}{\partial t} + (p_i - p_a) \sum_{n=1}^{\infty} \frac{\partial \bar{H}_{2n-1}(0)}{\partial t}. \tag{4-7}
 \end{aligned}$$

Performing the indicated operations and equating like terms of order $(2n - 1)$ yields,

$$\begin{aligned}
 \omega_{2n-1} &= \frac{8}{\pi^2(2n-1)^2} \\
 \lambda_{2n-1} &= \kappa - \alpha_{2n-1}^2 D\psi, \tag{4-8}
 \end{aligned}$$

with,

$$\psi = \frac{p_i - p_v}{p_i - p_a}. \tag{4-9}$$

Both Eqns. (3-26) and (4-6) have the same limits for large and small t , and the same derivative at $t = 0$.

Summary

Computational algorithms enjoy varying degrees of success and failure in decompression applications. More complex phase models address a greater number of issues, but are harder to program for general use. And the opposite is true for simpler supersaturation models. Exchange equations and decompression criteria are two distinct, but related, considerations. Exchange equations provide the vehicle to estimate tensions, apart from criticality. Decompression criteria set limits on levels of dissolved or separated gas in tissue, effectively dictating staging procedures. Both equations and criteria can be subjective in the absence of definitive data, the acquisition of which is tedious, sometimes controversial, and often ambiguous. Such subjectivity and leeway in parameter space can impart some commonality to computational algorithms, as seen, yet the range is not all inclusive. The bootstrap of Haldane half-lives to perfusion-diffusion parameters worked best for fast tissue compartments, while slow compartment M -values exhibited greater consistency with the phase criteria.

References

- 1 Boycott AE, Damant GCC and Haldane JS: The prevention of compressed-air illness, *J Hyg*, 8 (1908) 342—443.
- 2 Hempleman HV: *Investigation Into The Diving Tables: Basic Facts*, Medical Council Report UPS 168, London, 1957.
- 3 Behnke AR: The isobaric (oxygen window) principle of decompression, *Trans Third Annual Conf Marine Tech Soc*, 3, (1967) 1—27.
- 4 Bell RL and Borgwardt RE: The theory of high altitude correction in the US Navy standard decompression tables: I. The Cross corrections, *Undersea Biomed Res*, 3 (1976) 1—23.
- 5 Buhlmann AA: *Decompression/Decompression Sickness*, Springer-Verlag, Berlin, 1977.
- 6 Wienke BR: DECOMP: computational package for nitrogen transport modelling in tissues, *Comput Phys Commun*, 40 (1986) 327—336.
- 7 Wienke BR: Computational decompression models, *Int J Biomed Comput*, 21 (1987) 205—221.
- 8 Hennessy TR: The interaction of diffusion and perfusion in homogeneous tissue, *Bull Math Biol*, 36 (1974) 505—527.
- 9 Hennessy TR and Hempleman HV: An examination of the critical released gas concept in decompression sickness, *Proc R Soc London B*, 197 (1977) 299—313.
- 10 Hills BA: Linear bulk diffusion into heterogeneous tissue, *Bull Math Biophys*, 30 (1968) 47—59.
- 11 Hills BA: *Decompression Sickness*, John Wiley and Sons Inc., New York, 1977.
- 12 Irving IJ and Mullineux N: *Mathematics In Physics and Engineering*, Academic Press Inc., London, 1972.
- 13 Sagan H: *Boundary and Eigenvalue Problems In Mathematical Physics*, John Wiley and Sons Inc., New York, 1971.
- 14 Kety SS and Schmidt CF: The determination of cerebral blood flow in man by use of nitrous oxide in low concentrations, *Am J Physiol*, 143 (1945) 53—56.
- 15 Kety SS: Theory and applications of exchange of inert gases at lungs and tissues, *Pharmacol Rev*, 3 (1951) 1—41.
- 16 Krogh A: The rate of diffusion of gases through animal tissues, with some remarks on the coefficient of invasion, *J Physiol*, 52 (1945) 391.
- 17 Wienke BR: Tissue gas exchange models and decompression computations: a review, *Undersea Biomed Res*, 16 (1989) 53—89.
- 18 Workman RD: *Calculation Of Decompression Schedules For Nitrogen-Oxygen And Helium-Oxygen Dives*, USN Experimental Diving Unit Research Report, NEDU 6-65, Washington DC, 1965.
- 19 Schreiner HR and Kelley PL: A pragmatic view of decompression, *Proc Fourth Symp Underwater Physiol*, 1 (1971) 205—219.
- 20 Spencer MP: Decompression limits for compressed air determined by ultrasonically detected blood bubbles, *J Appl Physiol*, 40 (1976) 229—235.
- 21 Yount DE and Hoffman DC: On the use of a bubble formation model to calculate diving tables, *Aviat Space Environ Med*, 57 (1986) 149—156.